Asian Journal of Pharmaceutical Sciences 19 (2024) 100906

Available online at www.sciencedirect.com

ScienceDirect

journal homepage: www.elsevier.com/locate/AJPS

Research Article

Overcoming neutrophil-induced immunosuppression in postoperative cancer therapy: Combined sialic acid-modified liposomes with scaffold-based vaccines

*Cong Li, Lihong Wang, Kexin Zhang, Zeyu Wang, Zhihang Li, Zehao Li, Lijiang Chen**

School of Pharmaceutical Science, Liaoning University, Shenyang 110036, China

ARTICLE INFO

Article history:
Received 20 October 2023
Revised 13 January 2024
Accepted 17 February 2024
Available online 16 March 2024

Keywords:
Postoperative tumor treatment
Immunotherapy
Scaffold-based cancer vaccine
Inflammatory neutrophils
Sialic acid-modified liposome

ABSTRACT

Immunotherapy is a promising approach for preventing postoperative tumor recurrence and metastasis. However, inflammatory neutrophils, recruited to the postoperative tumor site, have been shown to exacerbate tumor regeneration and limit the efficacy of cancer vaccines. Consequently, addressing postoperative immunosuppression caused by neutrophils is crucial for improving treatment outcomes. This study presents a combined chemoimmunotherapeutic strategy that employs a biocompatible macroporous scaffold-based cancer vaccine (S-CV) and a sialic acid (SA)-modified, doxorubicin (DOX)-loaded liposomal platform (DOX@SAL). The S-CV contains whole tumor lysates as antigens and imiquimod (R837, Toll-like receptor 7 activator)-loaded PLGA nanoparticles as immune adjuvants for cancer, which enhance dendritic cell activation and cytotoxic T cell proliferation upon localized implantation. When administered intravenously, DOX@SAL specifically targets and delivers drugs to activated neutrophils *in vivo*, mitigating neutrophil infiltration and suppressing postoperative inflammatory responses. *In vivo* and *vitro* experiments have demonstrated that S-CV plus DOX@SAL, a combined chemo-immunotherapeutic strategy, has a remarkable potential to inhibit postoperative local tumor recurrence and distant tumor progression, with minimal systemic toxicity, providing a new concept for postoperative treatment of tumors.

1. Introduction

Surgery is the primary treatment for solid tumors, but it can leave residual tumor cells that may cause local relapse or distant metastases, leading to poor outcomes and high mortality rates [1,2]. Immunotherapy has shown great promise in various types of cancer and could be a potential approach to prevent postoperative tumor recurrence and metastasis [3–9], appears to be an attractive option for

* Corresponding author.
E-mail address: clj1172023@163.com (L. Chen).
Peer review under responsibility of Shenyang Pharmaceutical University.

https://doi.org/10.1016/j.ajps.2024.100906

inhibiting postoperative tumor recurrence and metastasis [10–12]. It has been reported that localized tumor vaccines can induce systemic antitumor immune responses with reduced systemic toxicity [13,14]. Recently, scaffold-based localized vaccine delivery platforms have been explored to introduce tumor antigens to dendritic cells (DCs) and trigger a robust antitumor immune response [15,16]. Implantable matrices fabricated with biocompatible and biodegradable materials, featuring porous structures, not only provide sustained release of immunomodulatory agents at residual tumor sites but also offer a residence and activity space for recruited and stimulated lymphocytes to interact with immunomodulatory agents [17,18]. Hyaluronic acid (HA) and collagen have been suggested as attractive materials for scaffold construction due to their immunoneutrality for clinical translation [19,20]. Whole tumor lysates are widely used as antigen sources to reflect the heterogeneity of tumors and stimulate antigen-presenting cells [21,22]. Immune adjuvants (such as TLR7 agonist R837) are also suitable for *in situ* administration to avoid cytokine storms upon systemic administration and enhance antitumor immune responses for inhibiting tumor recurrence [23,24].

During surgery, the tumor resection process can trigger a severe inflammatory response, characterized by the secretion of inflammatory cytokines such as IL-6, CXCL-1, IL-12, and TNF-α. These cytokines can recruit a large number of activated neutrophils to the inflamed tumor site [25,26]. However, studies have shown that this operation-induced inflammation can actually accelerate tumor regeneration and limit the effectiveness of cancer vaccines [27]. The infiltration of inflammatory neutrophils is often associated with the continuous recruitment of other immunosuppressive cells, enhanced angiogenesis, rapid tumor recurrence and metastasis, suppression of effector T cells, and a low response rate to tumor immunotherapy [28–30]. Therefore, it is crucial to design a drug delivery system that specifically targets inflammatory neutrophils, effectively reduces neutrophil recruitment, and inhibits neutrophil accumulation at the postoperative tumor site. This approach can help alleviate the immunosuppression associated with postoperative inflammation and significantly improve the treatment outcome of localized tumor vaccines [31,32].

L-selectin (CD62L) is an adhesion protein that is highly expressed on the membranes of peripheral neutrophils stimulated by inflammation. It plays a key role in neutrophil migration after inflammation activation [33]. Sialic acid (SA) is an endogenous ligand for L-selectin and can be used to modify drug carriers for targeted delivery to inflammatory neutrophils [34–36]. Doxorubicin (DOX), a classic cytotoxic antitumor agent, has been shown to induce neutrophil apoptosis at low doses, thereby suppressing neutrophil migration and inhibiting the postoperative inflammatory response [37,38]. Liposomes, which have excellent biocompatibility and biodegradability, can be easily decorated with functional ligands, making them ideal drug carriers for targeting neutrophils with DOX [39–41]. In order to balance the safety and anti-metastatic ability of postoperative tumor treatment, systemic administration of DOX@SAL (DOX, 0.5 mg/kg) was chosen for our study, unlike DOX at a conventional chemotherapeutic dose of 5 mg/kg [42].

The aim of this study was to innovate postoperative cancer immunotherapy to reduce postoperative tumor recurrence by enhancing antitumor immunity (Scheme 1). A biocompatible macroporous scaffold-based cancer vaccine (S-CV) containing whole tumor lysates as antigens and R837-loaded PLGA nanoparticles (R837@PLGA) as immune adjuvants was firstly prepared for postoperative cancer immunotherapy. After local implantation, immunotherapeutic agents (antigen and R837) were sequentially released from the scaffolds, which triggered an efficient antitumor immune response and enhanced the activation of DCs and proliferation of cytotoxic T cells. The DOX-loaded liposome platform (DOX@SAL) was further modified by an SA derivative (SA-PG-C18) to target activated neutrophils at the tumor site, effectively reducing inflammation and restoring postoperative immune homeostasis. The two strategies work synergistically to exert highly potent postoperative local and distant tumor metastatic inhibitory activity while minimizing systemic toxicity. Compared with existing immunotherapies, this study proposes a novel neutrophil-targeted nano-delivery system, which provides a new strategy for overcoming postoperative immunosuppression, improving the efficacy of local immunotherapy, and providing a combined treatment strategy to address postoperative tumor recurrence and metastasis. This integrated strategy represents a new advancement in addressing the complexities of postoperative cancer therapy.

2. Material and methods

2.1. Materials, cells and animals

2.1.1. Materials

TLR7 agonist (R837), poly(D, L-lactic co-glycolic acid) (PLGA), polyvinyl alcohol (PVA), EDC/NHS and DAPI were provided by Sigma-Aldrich (St. Louis, USA). Hyaluronic acid (HA, MW = 50 kDa) were obtained from Bloomage Biotech Co., Ltd (Jinan, China). Type I collagen, hyaluronidase and collagenase D were supplied by Meilunbio Co., Ltd (Dalian, China). HSPC and CH were provided by AVT (Shanghai) Pharmaceutical Tech Co., Ltd. DOX (purity 99.0%) was supplied by Olympic Star Pharmaceutical Co., Ltd (Shenzhen, China). Poly(glycerin)10-monostearate (PG-C18) was supplied by Shandong Binzhou GIN&ING New Material Technology Co., Ltd. (Shandong, China). SA was provided by Changxing Pharmaceutical Co. Ltd (Huzhou, China). RPMI 1640 medium, FBS and penicillin-streptomycin solution were provided by Gibco (Carlsbad, USA). PE-CD11c, APC-CD40, APC-CD80, FITC-Gr-1, APC-CD86, FITC-CD3, PerCP-CD4 and APC-CD8 antibodies were obtained from eBioscience (San Diego, USA). ELISA kits of IL-6, IL-12, TNF-α, CXCL1, CCL2, IFN-γ, TGF-β and Arg-1 were supplied by R&D Systems (Minneapolis, USA). anti-CD62L, anti-MMP-9 and anti Arg-1 antibodies were supplied by BioXCell (West Lebanon, USA). Cell Counting Kit-8 (CCK-8) was obtained from Dojindo Laboratory (Kumamoto, Japan). All the other materials were immediately applied as supplied.

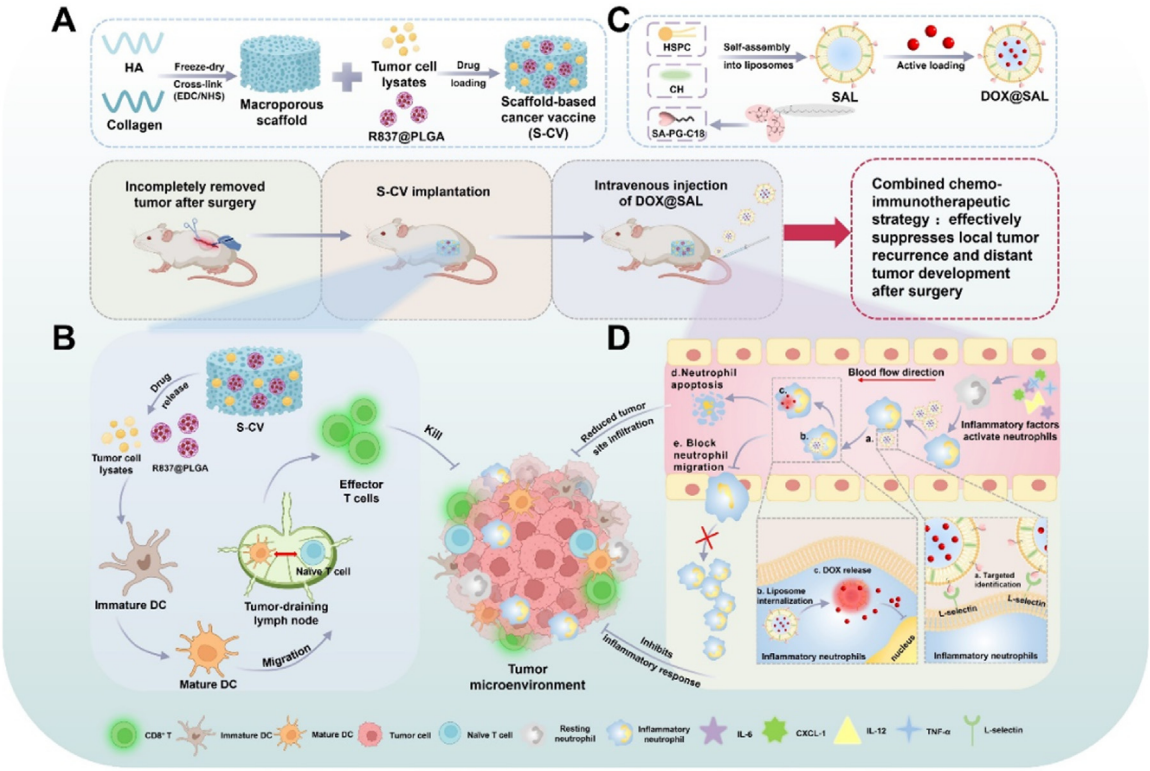

Scheme 1 – The combination therapy for postoperative tumor treatment. (A-B) S-CV containing tumor lysates and R837@PLGA is implanted locally, enhancing DC activation and cytotoxic T cell proliferation. (C-D) DOX@SAL is administered intravenously, targeting and delivering drugs to activated neutrophils, mitigating neutrophil infiltration and suppressing postoperative inflammatory responses. The combination of these therapies effectively suppresses local tumor recurrence and distant tumor development after surgery with minimal systemic toxicity.

2.1.2. *Cells and animals*

The 4T1 murine breast cancer cell lines were obtained from the Cell Bank of the Chinese Academy of Sciences in Shanghai, China, and cultured in complete RPMI 1640 medium supplemented with 1% penicillin-streptomycin and 10% FBS. The cell cultures were grown in a 5% CO_2 atmosphere at 37 °C. Female BALB/c mice, weighing 20 ± 2 g and aged 6–7 weeks, were obtained from Liaoning Changsheng Biotechnology Co., Ltd. in Shenyang, China. All animal procedures were conducted in compliance with the guidelines of the Animal Care & Welfare Committee of Liaoning University. To establish the post-surgical mouse model and implant scaffold [35], 1×10^6 4T1 tumor cells were inoculated subcutaneously into the right mammary fat pad of female BALB/c mice. When the tumors reached approximately 200 mm^3 in size, the tumor-bearing mice were anesthetized using a 2.5% solution of 2,2,2-tribromoethanol. The operative sites were sterilized with 70% ethanol, and approximately 90% of the tumor tissues were excised. During the operative procedure, scaffold-based cancer vaccines were implanted next to the tumor tissues.

2.2. *Fabrication and characterization of S-CV*

2.2.1. *Production of 4T1 tumor cell lysates*

To prepare the tumor antigen, the cultured 4T1 cells were digested and suspended in fresh PBS at a cell density of 1×10^7 (1 ml). Next, they were quickly immersed in liquid nitrogen and then warmed at 37 °C for 5 cycles. Following centrifugation at 500 g for 10 min, the supernatant containing the tumor cell lysates was harvested, and protein levels were quantified through a Bicinchoninic acid (BCA, Beyotime) test.

2.2.2. *Preparation and characterization of R837@PLGA*

R837@PLGA or FITC-labelled R837@PLGA nanoparticles were synthesized using a conventional oil/water emulsion method [43]. Firstly, R837 was solubilized in DMSO to achieve a concentration of 2.5 mg/ml and mixed with 1 ml of PLGA (or FITC-PLGA) dissolved in dichloromethane at 5 mg/ml. Next, the mixture was preliminarily emulsified using a probe sonicator for 5 min with 2 ml of 5% PVA solution. The resultant oil/water emulsive mixture was slowly supplemented dropwise into 5% PVA solution (8 ml). After the organic solvent was evaporated at ambient temperature for 12 h, the R837@PLGA or FITC-labelled R837@PLGA nanoparticles were gathered through the process of centrifugal separation at 4,000 g for 30 min.

The structural characteristics of nanoparticles were examined with a JEOL JM-1200EX transmission electron microscope (TEM, Tokyo, Japan). The nanoparticles were positioned on a 300-mesh copper grid and subjected to negative staining using a 1.0% solution of phosphotungstic acid to prepare TEM samples. The dynamic diameters of

nanoparticles were characterized using the NICOMP™ 380 particle sizing system. The efficiency of encapsulation (EE%) for R837 was evaluated through an HPLC system (Elite Analytical Instruments Co., Ltd., Dalian, China) using acetonitrile as the mobile phase at 325 nm.

2.2.3. *Fabrication and characterization of S-CV*

HA/collagen matrices were fabricated through a lyophilization process [44]. Firstly, HA (MW = 50 kDa) and type I collagen were dispersed in PBS, and each dispersion was mixed until the weight ratios of HA/collagen were 8/2, 5/5 and 2/8, respectively. The blend was agitated at 300 rpm for two h at 4 °C. Next, 250 µl of the resulting mixture suspension was poured into a PDMS mold (with a thickness of 2 mm and a diameter of 8 mm). To improve the physical stability, provide a porous structure, and increase crosslinking efficiency of scaffolds, the blends were subjected to freezing at −20 °C for 12 h followed by lyophilization at −80 °C for an additional 12 h. For crosslinking, the lyophilized scaffolds were immersed in 20 mM NHS and 50 mM EDC dissolved in 95% ethanol and shaken under ambient conditions for 24 h. The prepared matrices were carefully withdrawn and thoroughly washed with distilled water, then re-frozen and re-lyophilized using the aforementioned conditions.

The morphologies of the porous scaffolds fabricated with different HA/collagen ratios were imaged utilizing a JEOL Ltd JSM 7000F scanning electron microscope (SEM, based in Tokyo, Japan). To prepare SEM specimens, platinum was applied to the cross-sections of the freeze-dried structures by sputter coating. The pore zones of the scaffolds were measured using an ImageJ 1.48 analysis program, and the mean diameter of pores was assessed by measuring at least 30 random pores.

To encapsulate tumor antigens and immune adjuvants into the scaffolds, 4T1 cell lysates (500 µg protein per scaffold) and R837@PLGA nanoparticles (100 µg R837 per scaffold) were uniformly dropped onto the scaffolds, followed by a 12-h incubation at a temperature of 4 °C before implantation into the tumor removal cavity.

2.2.4. *In vitro enzymatic degradation study*

To investigate the *in vitro* degradation behavior of S-CV, cross-linked scaffold samples were incubated with 1 ml of RPMI 1640 only, or RPMI 1640 containing hyaluronidase (100 µg/ml) and collagenase D (100 µg/ml) at a steady temperature of 37 °C with continuous agitation at a speed of 50 rpm. The scaffold specimens underwent triple rinsing with purified water, lyophilized, and the masses of the residual structures were documented at specific time intervals.

2.2.5. *In vitro drug release study*

S-CV were incubated in PBS (1 ml) per well, agitated at a temperature of 37 °C and a speed of 50 rpm. At specified time intervals, the drug release solution was collected from each well and supplemented with fresh media. The released tumor cell lysate was detected using a BCA protein test. The amount of FITC-labelled R837@PLGA released was measured utilizing a spectrophotometric plate reader, set to detect at specific wavelengths: 490 nm for excitation and 520 nm for emission.

2.3. *Preparation and evaluation of DOX@SAL*

2.3.1. *Synthesis of SA conjugate*

The SA conjugate (SA-PG-C18) was synthesized using EDC/NHS as catalysts between SA and PG-C18. Initially, SA (containing 10 mmol -COOH), PG-C18 (0.5 mmol), EDC (4 mmol), and NHS (2 mmol) were dissolved completely in anhydrous formamide (7 ml) in a nitrogen environment. The reaction blend was agitated at ambient temperature for a duration of 30 min, following which TEA (4 mmol) was supplemented dropwise into the reaction system and agitated for an extra 8 h. The reactants were then collected and subjected to dialysis (MWCO = 10 kDa) against distilled water for a period of 24 h. The purified SA-PG-C18 was analyzed using FTIR (Nexus-470, Nicolet, USA) and ^{1}H NMR (Avance III 400 MHz, Bruker, Switzerland).

2.3.2. *Preparation of DOX-loaded liposomes*

Blank liposomal preparations were constructed by a modified lipid film-rehydration technique [45]. SA-modified empty liposomes (SAL) were consisting of HSPC/CH/SA-PG-C18 in a molar ratio of 55:40:5, while unmodified empty liposomes (CL) were consisting of HSPC/CH in a molar ratio of 55:45 to serves as a control for evaluating the effectiveness of DOX@SAL in targeting neutrophils and tumor treatment. The prescribed lipid material was solubilized in ethanol and stirred at 65 °C to evaporate most of the ethanol. Subsequently, citrate solution (pH 4.0, 200 mM) was introduced into the prepared lipid film and hydrated under stirring at 65 °C for 20 min. The prepared polydisperse liposomal particles were successively extruded through 0.8 µm twice, 0.45 µm twice, and 0.22 µm twice using polycarbonate membranes under nitrogen pressure to obtain empty liposomes with appropriate and uniform particle sizes. Maintaining nitrogen pressure in liposome extrusion through a regulated nitrogen supply and pressure monitoring ensures process stability, oxidation prevention, and temperature control.

To load DOX into the empty liposomes, a specific volume of sodium phosphate medium (500 mM) was evenly mixed with the prepared liposomal suspension to establish an ion gradient. Afterward, the DOX drug solution was added to the liposomes at a drug-to-phospholipid ratio of 1:10 (w/w). The mixture was subjected to incubation at 60 °C for a duration of 20 min, followed by stopped drug loading using an ice water bath to obtain DOX@SAL (the entrapment of DOX within liposomes modified with SA) and DOX@CL (the entrapment of DOX within liposomes without SA modification).

2.3.3. *Assessment of liposomal DOX*

The morphologies of DOX@SAL and DOX@CL were imaged using a JM-1200EX TEM. The zeta potential and particle dimensions of DOX@CL and DOX@SAL were characterized using the NICOMP™ 380 particle sizing system. The EE% of liposomal DOX was assessed utilizing a UV-1801 ultraviolet-visible spectrophotometer at a wavelength of 480 nm after dissolution with methanol.

To investigate the DOX release patterns of different preparations, DOX@SAL, DOX@CL, and free DOX were inserted into dialysis bags (MWCO = 10 kDa). The release medium

chosen was PBS (pH 7.4, 100 ml) to meet the sink condition, and the system was continuously agitated at 37 °C to simulate the physiological environment. At specified time intervals, the released drug solution was collected and supplemented with fresh media. The concentration of release DOX was quantified using a Bio-Rad Laboratories (located in Hercules, CA, USA) Model 650 microplate reader at 480 nm.

2.4. Isolation of bone marrow-derived cells (BMDCs)

Both the femurs and tibiae of rodents were harvested, and all bone ends were cut to expose the marrow cavity. The marrow cells were then flushed out utilizing RPMI 1640 medium, and erythrocytes were lysed. After differentiation for 7 d in RPMI 1640 medium supplemented with 1% penicillin-streptomycin, 20 ng/ml of GM-CSF and 10% FBS at 37 °C in a 5% CO_2 environment, the BMDCs were gathered for further studies.

2.5. In vitro activation and maturation of BMDCs by cancer vaccines

BMDCs were placed in 6-well plates at a density of 1×10^6 cells per well and treated using nanoparticulate immune adjuvants (10 μg/ml R837), 4T1 cell lysates, or both for 24 h at 37 °C. The liquid fractions were harvested, in addition to the concentrations of cytokines (TNF-α and IL-6) secreted from activated BMDCs were assessed employing ELISA kits following the manufacturer's guidelines

The maturation of BMDCs in response to tumor antigen and R837@PLGA was investigated using a Beckman Coulter FC500 flow cytometer (CA, USA). The indicated cell samples were labeled with PE-CD11c, APC–CD40, and APC–CD80 anti-mouse fluorescence-conjugated antibodies for 1 h at 4 °C. The percentages of $CD11c^+CD40^+$ and $CD11c^+CD80^+$ cells were recorded.

2.6. Extraction and characterization of inflammatory neutrophil cells

Neutrophil cells were harvested and purified from healthy mice and postoperative mice with 4T1 tumors employing a density gradient centrifugation method [46]. In brief, fresh blood was collected from rodent specimens and then transferred into heparinized tubes. An equal volume of red blood cell sedimentation fluid (HES-TBD550–80, TBD Science) was introduced, and the blend was permitted to rest at ambient temperature for 1 h. The white blood cell suspension was collected from the supernatant and added carefully onto 100% and 80% (1/2, v/v) mouse neutrophil isolation solution (TBD Science). After rotational separation for 20 min at 800 g, neutrophils were gathered from the medium interface, washed thrice with fresh PBS, and quantified using a hemocytometer. The purity of neutrophils was assessed using an FC500 flow cytometer after staining with FITC-Gr-1 antibody.

The level of L-selectin (SA-binding receptor) on neutrophil cell membranes was evaluated using a western blot study. Neutrophils were isolated from healthy and postoperative mice, lysed, and the obtained protein specimens underwent separation via SDS-PAGE and were subsequently conveyed onto PVDF membranes. The proteins were examined using primary antibodies for β-actin and L-selectin (Biolegend), next stained using horseradish peroxidase-conjugated secondary antibody (Biolegend) and visualized by a MicroChemi 4.2 Gel Imaging System (manufactured by DNR, Israel).

2.7. In vitro neutrophil uptake behavior

CLSM and FCM were utilized to investigate the internalization of liposomal DOX by inflammatory neutrophils from post-surgical mice. For FCM, neutrophil cells (2×10^5 per milliliter) were seeded into 6-well culture plates, then stabilized in RPMI 1640 medium without FBS for 1 h at 37 °C. Afterwards, DOX@SAL and DOX@CL (DOX, 10 μg/ml) were introduced into the culture medium, then cultured for another 30 min. For the study involving competitive inhibitors, neutrophils subjected to pretreatment with anti-L-selectin (CD62L) antibody to pre-saturate the SA-binding receptors on cell membranes, then cultured with DOX@SAL [referred to as the DOX@SAL (aCD62L)]. Next, the cells underwent thrice rinses using fresh PBS, evaluated utilizing a flow cytometer, and analyzed using FlowJo 10.8.1 software.

For CLSM, 6-well plates containing glass coverslips were populated with neutrophils with a density of 2×10^5 cells/ml, subsequently subjected to DOX formulations as previously mentioned. The neutrophils were then marked using DAPI (50 μl/well) to label the cell nucleus. The prepared cell slides were subjected to fixation using 4% paraformaldehyde, then analyzed using an LSM 800 CLSM (Zeiss, Germany).

2.8. In vitro neutrophil inhibition study

The apoptosis of neutrophils induced by DOX formulations was investigated by a CCK-8 assay. Neutrophils (2×10^5 cells/ml) isolated from post-surgical mice were cultured in RPMI 1640 medium without FBS at a temperature of 37 °C for a duration of 1 h in 96-well plates. DOX-S, DOX@SAL, and DOX@CL at different ultimate concentrations of 0, 2.5, 5, 10 and 20 μg/ml were introduced into the plate and cultured for another 1 h. Blank wells (without cells and drugs), as well as control wells (without drugs with cells) were also established. Finally, CCK-8 solution (10 μl/well) was introduced into the medium, then cultured for a period of 4 h. The cell viability (%) was determined employing a microplate spectrophotometer set to absorbance at 480 nm.

The inhibition of neutrophil migration induced by DOX preparations was assessed using a Transwell migration test employing a PC membrane equipped with a pore dimension of 0.33 cm^2. First, inactivated and activated neutrophils (2×10^5 cells/ml) were treated with different DOX preparations at 37 °C for 30 min with a concentration of 10 μg/ml to obtain the neutrophils with internalized DOX formulations. Subsequently, neutrophils (2×10^5 cells/well) with or without DOX formulations were seeded on the upper chamber. FBS-excluded RPMI 1640 medium with an additional 10 nM fMLP was introduced into the lower chamber to simulate the inflammatory postoperative tumor microenvironment. After 1 h of migration, the culture medium in the lower wells was gently collected, as well as the quantity of harvested neutrophils was enumerated with a hemocytometer.

2.9. *In vivo study of cytokine secretion after surgery*

In order to implant the scaffold in the postoperative site of mice, the mice were first anesthetized and placed under an infrared lamp to maintain body temperature. The surgical area was shaved and sterilized to create a sterile operating environment. Approximately 90% of the tumor tissue was excised to simulate the clinical scenario, and an appropriate incision was made to accommodate the scaffold. Subsequently, the pre-prepared scaffold was carefully placed into the created space, ensuring its proper positioning and good alignment with the surrounding tissues to avoid displacement. Finally, the surgical incision was carefully sutured to ensure proper closure and minimize the risk of infection. The cytokine secretion in the tumor site and serum of surgically treated mice after scaffold implantation was studied via an ELISA assay. The regrown neoplastic specimens were harvested, then homogenized on Day 5, 7, 14 and 30 after surgery. Blood samples were also collected at different times, then serum was acquired by a centrifugation at 500 g for a duration of 10 min. The concentrations of TNF-α, CXCL1, and CCL2 in the serum, as well as IL-12 and IL-6 in the residual neoplasm homogenate, were measured utilizing ELISA kits in accordance with the manufacturer's guidelines.

2.10. *In vivo study of immune cell recruitment into scaffolds*

Post-surgical BALB/c mice were subcutaneously implanted with either cancer vaccine-loaded scaffolds or blank scaffolds. The mice were euthanized upon reaching a significant weight loss of 20%−25%. The frameworks were gathered on Days 5, 7, 14 and 30 after surgery, and the resulting regrown tumor tissues were minced into small pieces, then subjected to collagenase D treatment (1 mg/ml) within RPMI 1640 media under shaking for 1 h at 37 °C. The cell suspensions were sieved through nylon meshes (70 μm), treated with erythrocyte lysing buffer for 10 min at 37 °C, and rinsed thrice using fresh PBS. All recruited immune cells were labeled using PE-CD11c, as well as APC-CD86 antibodies to label DCs, and FITC-Gr-1 antibody to label neutrophils. The prepared specimens were analyzed using a flow cytometer.

2.11. *Antitumor effect of S-CV plus DOX@SAL treatment*

To explore the anti-cancer activity of postoperative immunotherapy, 4T1 mouse models with tumors were randomly allocated into seven categories ($n = 8$ per category). After tumor resection and further treated with 5% Glu (control), blank scaffolds, scaffolds loaded with tumor lysates and R837@PLGA (S-CV), DOX@CL, DOX@SAL, S-CV plus DOX@CL, or S-CV plus DOX@SAL (DOX with 0.1 mg/ml concentration and 0.5 mg/kg dosage). Any mice showing unusually fast or slow tumor growth were excluded from the study prior to random grouping and surgery.

The accurate liposomal dilution for injection involves removing unencapsulated DOX with a cationic fiber column, determining drug concentration via UV spectrophotometry at 480 nm, and adjusting to the desired concentration using 0.9% NaCl as the diluent. Scaffolds containing 500 μg tumor lysate protein per mouse and 100 μg R837 per mouse were implanted during the operative process. DOX@CL and DOX@SAL received intravenous injection with an identical DOX dosage of 0.5 mg/kg once every 3 d after surgery. The post-surgical tumor-bearing mice were euthanized on Day 7 and 14 after tumor resection. Neoplasm specimens were excised, weighed, and subdivided for flow cytometry, immunofluorescent staining, and ELISA tests. Regrown tumor tissues were prepared as mentioned above to obtain individual cell dispersions, which were then labelled using FITC-Gr-1 antibody for inflammatory neutrophils, PE-CD11c and APC-CD86 antibodies for DCs, as well as FITC-CD3, PerCP-CD4, and APC-CD8 antibodies for T cells. The frozen neoplasm slices, which had been readied in advance, were exposed to antibodies targeting MMP-9 and Arg-1, then made visible using fluorescence microscopy. The intratumoral production of IFN-γ and TGF-β cytokines was determined using specific ELISA kits in accordance with the guidelines provided by the manufacturer. The draining lymph nodes and spleens were also harvested, ground by syringe pistons, filtered through 70 μm nylon meshes, and treated with erythrocyte lysing buffer for the purpose of FCM examination. The obtained lymphatic cells and splenocytes were stained with fluorescence-conjugated antibodies to label DCs and T cells, respectively.

A separate experiment was carried out to assess the anti-metastatic efficacy of postoperative combined immunotherapy. 4T1 mice with tumors ($n = 8$ in each category) were administered using different treatment regimens and were euthanized on Day 28 following tumor removal. The lungs were harvested, weighed, as well as the number of metastatic malignancy nodules was tallied. The harvested lung, liver, heart, kidney and spleen specimens were immersed into paraffin, sectioned, then subjected to H&E staining for histopathological assessment. For the extended-term survival study, postoperative mice with 4T1 tumors were treated using the various treatment groups as described above. Their weights were observed every second day, and the survival outcomes were presented using a Kaplan–Meier curve.

2.12. *Statistical assessment*

The study findings are displayed as average ± standard deviation (SD). Statistical significance among sample categories was calculated through the two-tailed Student's *t*-test, else one-way analysis of variance (ANOVA), and significance was determined at $P < 0.05$. Software (GraphPad Prism) was applied in all statistical assessments.

3. Results and discussion

3.1. *Fabrication and characterization of S-CV*

The implantable porous scaffolds were composed of HA and collagen, which are primary components of the extracellular matrix, making them highly biodegradable and biocompatible (Fig. 1A). The scaffolds were fabricated in three steps: (i) HA and collagen were mixed at various ratios, (ii) the mixed

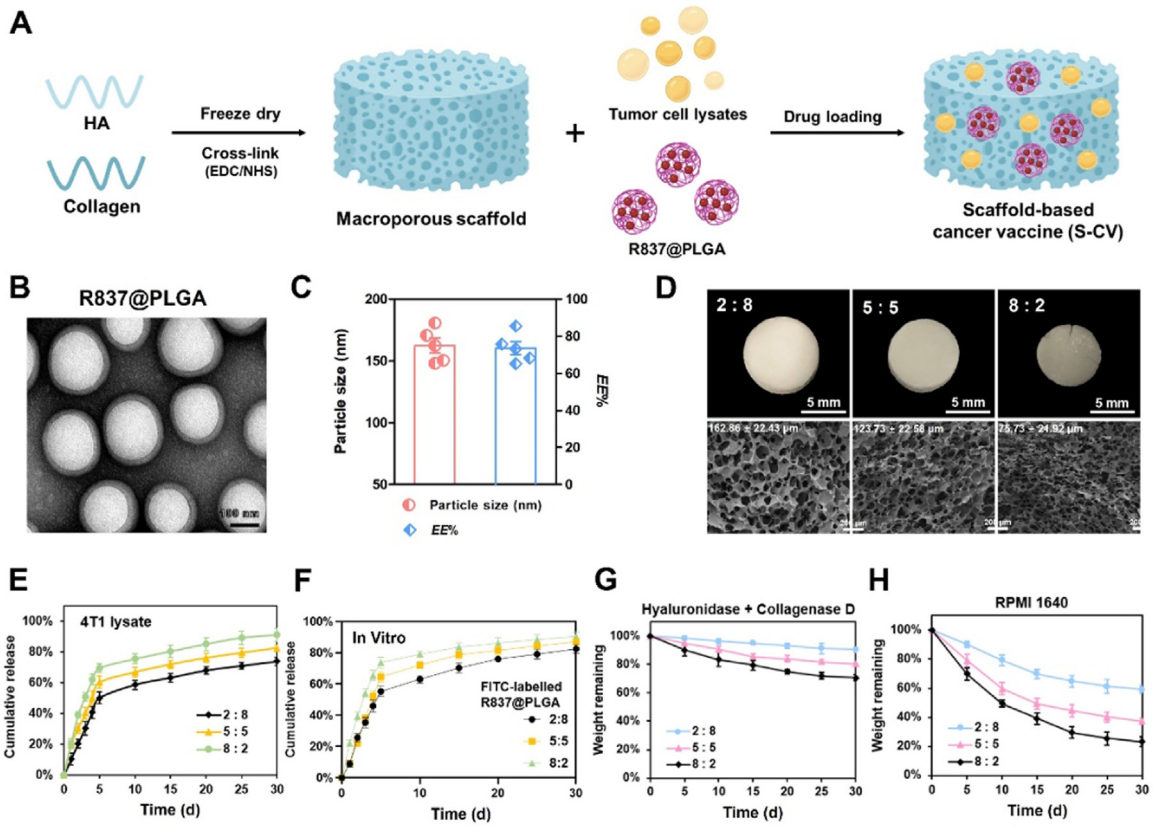

Fig. 1 – Formation and assessment of S-CV. (A) Graphic depiction of S-CV formation procedure; (B) TEM image of R837@PLGA, scale bar = 100 nm; (C) Particle size and EE% of R837@PLGA; (D) Optical imaging (scale bar = 5 mm) and sSEM imaging (scale bar = 200 μm) of porous scaffolds prepared using various HA/collagen mass ratios; *In vitro* cumulative release of (E) 4T1 lysate and (F) R837 from matrices featuring diverse HA/collagen mass proportions; *In vitro* degradation kinetics of matrices featuring diverse HA/collagen mass proportions in (G) RPMI 1640 and (H) in RPMI 1640 containing hyaluronidase (100 μg/ml) and collagenase D (100 μg/ml). Data are mean ± SD, *n* = 5.

solutions were slowly frozen and lyophilized to generate a networked porous structure, and (iii) the created matrices were cross-linked using water-soluble EDC/NHS to maintain stability. The morphology of the matrices was analyzed by photographic and SEM micrographs. In accordance with Fig. 1D, the cross-section of the scaffold exhibited evenly spread and interlinked macroporous network with pore dimensions ranging from 162.86 ± 22.43 to 75.73 ± 21.92 μm, depending on the blended ratio of HA/collagen. Implantable scaffolds used for cancer vaccines must possess an adequate pore size to accommodate large amounts of immune cells [47]. A minimum collagen content of 50% was used to form scaffolds that maintain a stable and highly porous structure.

The drug loading and release behavior of 4T1 tumor antigens and adjuvants were also taken into account when determining the ideal HA/collagen blend ratio to trigger efficient antitumor immune responses [48]. Imiquimod (R837) was chosen as the immune adjuvant, which is known to activate TLR7 in DCs and initiate a robust immune response. R837@PLGA nanoparticles (with a size of 162.58 ± 13.70 nm and EE% of 73.62% ± 7.83%) were prepared and incorporated into scaffolds to improve free R837 solubility, enhance phagocytosis by immune cells, and enabling a prolonged, uniform drug release [24,49-51] (Fig. 1B and 1C). Due to the swelling potential of HA, the tumor cell lysate and nanoadjuvant suspensions can be readily absorbed into lyophilized scaffolds without significant drug leakage after loading. Generally, immune cells, including DCs, rapidly increase during the early stage of tumor resection and regrowth due to the inflammatory effect [52]. As illustrated in Figs. 1E, 1F, S1 and S2, with a HA/collagen ratio of 5:5, approximately 60%–80% of proteins and nucleic acids from tumor cell lysates, as well as FITC-labelled R837@PLGA nanoadjuvants were released within the first 5 d, which activated infiltrated DCs, as well as initiated the antitumor immunity reactions. The remaining therapy agents were sustained released from the matrix over a period of 30 d, promoting the activation and enrichment of DCs over an extended time. These release profiles are likely attributed to the hydrophobic interaction and electrostatic repulsion between drugs and the matrix.

It is crucial to emphasize that the degradation behavior of the scaffolds can also be modified by adjusting the ratio of HA and collagen [53]. When exposed to hyaluronidase and collagenase D, the S-CV formulated with a HA/collagen ratio of 5:5 exhibited sustained and substantial degradation within 30 d, allowing for spatiotemporal regulation of the

immunosuppressive microenvironment in the tumor surgical site (Fig. 1G and 1H).

3.2. *Production and analysis of DOX@SAL*

DOX@SAL liposomes were fabricated to specifically target and suppress inflammatory neutrophils with the objective of decreasing postoperative inflammation, as well as improving the effectiveness of immunotherapy (Fig. 2A). To achieve this, a SA derivative was synthesized by covalently conjugating the carboxylic fragment of the SA targeting ligand with the hydroxyl fragment of the PG-C18 liposomal anchor. The structure of SA-PG-C18 was characterized using FT-IR and ^{1}H NMR analyses (Fig. S3).

As shown in Fig. 2B, TEM images show that liposomal DOX is spherical with a representative double-layer

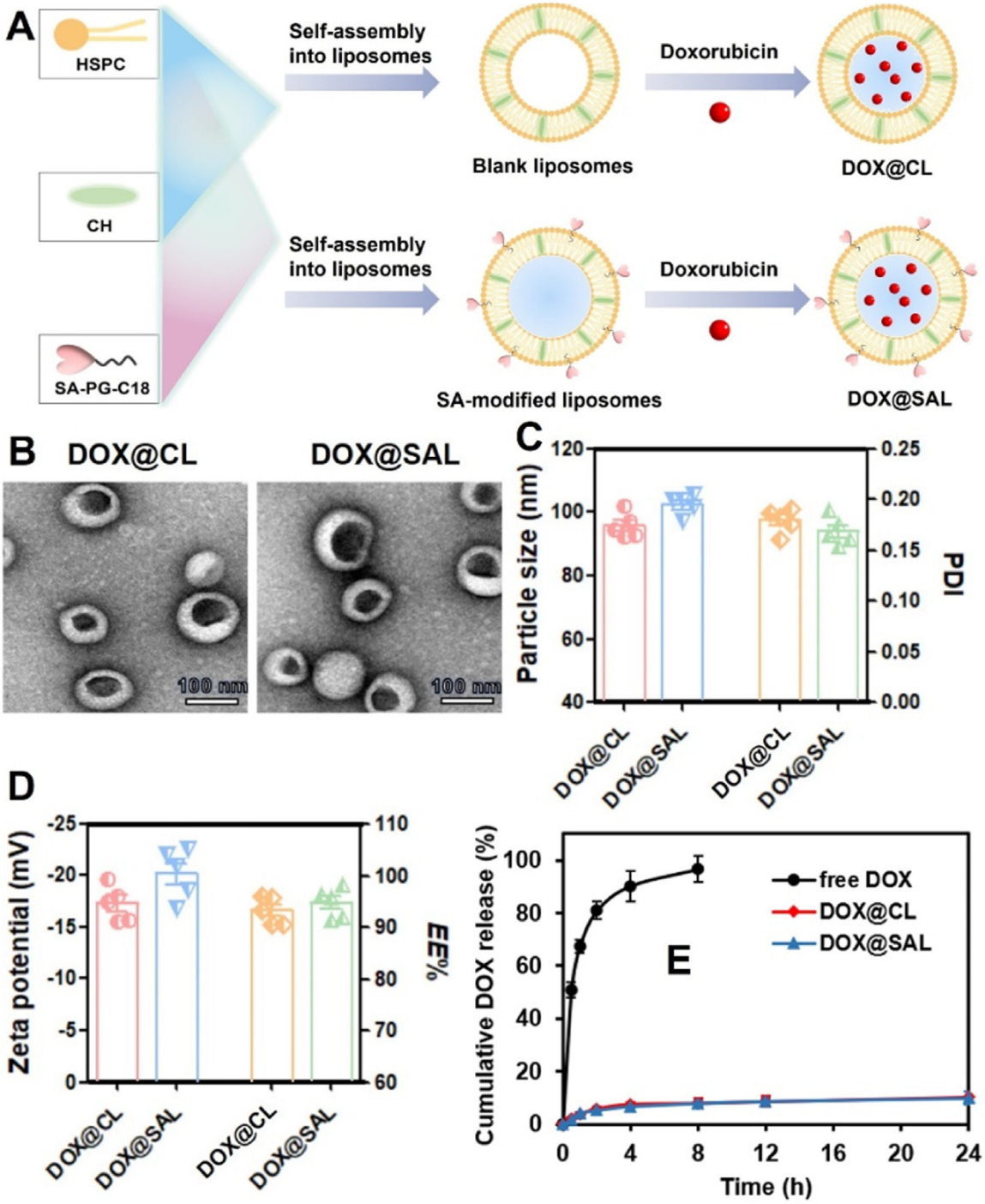

Fig. 2 – Creation and analysis of liposomal DOX. (A) Formulation of liposomal DOX; (B) TEM pictures of various liposomal formulations (scale bar = 100 nm); (C) Particle dimensions and PDI, as well as (D) zeta charge and EE% of DOX@SAL and DOX@CL; (E) *In vitro* DOX release from different preparations in physiological settings. Results are mean ± SD, $n = 5$.

phospholipid structure and a homogeneous size distribution. Dynamic light scattering examinations Uncovered that the sizes of DOX@SAL and DOX@CL were 102.43 ± 6.58 nm (PDI = 0.169 ± 0.019) and 95.7 ± 4.0 nm (PDI = 0.175 ± 0.017), respectively, which plays a crucial role in the stability, cell internalization and biodistribution of liposomes [54]. The zeta potentials of DOX@SAL and DOX@CL were −20.1 ± 2.4 mV and −17.3 ± 1.7 mV, respectively, preventing particle aggregation and agglomeration for improved stability and biocompatibility [55]. DOX@SAL and DOX@CL showed extremely high efficiencies of DOX encapsulation (%) of 93.3% ± 2.7% and 94.8% ± 2.9%, respectively (Fig. 2C and 2D).

The *in vitro* release characteristics of DOX formulations were examined using dialysis under physiological, as well as endosomal conditions, as shown in Fig. 2E. DOX solution still has a release profile within 8 h perhaps due to the properties of dialysis membrane, the gradually decreasing concentration gradient. Compared to DOX solution, both liposomal DOX formulations exhibited significantly lower drug release rates, with only about 10% of the drug released within 24 h, and with only about 30% of the drug released within 72 h under physiological conditions. In addition, the DOX release behavior of DOX@CL and DOX@SAL significantly increased to almost 60% within 72 h under conditions of pH 5.5 and high enzyme content (Fig. S4).

Moreover, there was no noteworthy contrast in the release profiles between DOX@CL and DOX@SAL, indicating that the SA-PG-C18 decoration possessed no impact on the release properties of the liposomes. These results demonstrated the effective drug storage capability of the liposomal carriers, which could potentially avoid the acute toxicity of free drugs, and further highlighted the capability of DOX@SAL in future research.

3.3. *Therapeutic agents loaded in S-CV can activate and mature BMDCs in vitro*

The *in vitro* immunostimulatory effects of the antigens and immune adjuvants released from S-CV were evaluated by their ability to activate and mature BMDCs. Activated and matured DCs are characterized by their expression of costimulatory markers, including CD40 and CD80, which allow them to trap, handle, and display antigens to effector T cells [56]. FCM examination indicated that the combination treatment of 4T1 neoplasm lysates and R837@PLGA nanoparticles significantly upregulated the expression levels of CD80 and CD40 surface markers upon BMDCs, compared to either treatment alone or blank controls (Figs. 3A, 3B and S5). Additionally, the combined therapy significantly increased the secretion of TNF-α and IL-6, which are produced by matured BMDCs and stimulate the growth and initiation of effector T cells [57]. The results illustrate that the co-treatment of tumor antigens and TLR7 agonists can strongly enhance the function of BMDCs (Fig. 3C and 3D).

3.4. *In vitro targeting and inhibition of inflammatory neutrophils by liposomal DOX*

Normal and inflammatory neutrophils were enriched and purified from murine peripheral blood using density separation by centrifugal force. The neutrophil output amounted to around 6×10^5 cells per mouse, and the purity of neutrophils was determined using FITC-Gr-1 antibody immunofluorescence staining, which revealed that neutrophil purity was greater than 90% (Fig. 3E). Western blotting examination results indicated that the L-selectin expression amount, which upregulates during inflammatory responses and mediates selective uptake of SA-modified formulations. As shown in Fig. 3F and S6. L-selectin expression on the surface of neutrophil cells was slightly higher in unoperated mice with neoplasm than in healthy mice, whereas the L-selectin expression on the surface of neutrophils in operated mice with neoplasm was noticeably greater than that in normal mice and unoperated mice with neoplasm. The results suggest that the neutrophils obtained from mice after surgery predominantly exhibited an inflammatory phenotype and were appropriate for further cellular investigations.

The *in vitro* selective internalization of SA-modified liposomal DOX by inflammatory neutrophils was evaluated using FCM and CLSM. As shown in Fig. 3G and 3H, the SA-PG-C18 decoration significantly enhanced the internalization of liposomal DOX by neutrophil cells. The DOX fluorescence intensity of SA-modified liposomes was 278% higher than that of conventional liposomes. We further investigated the uptake behavior of inflammatory neutrophils when the SA-binding receptors on neutrophil membranes were pre-saturated with anti-mouse CD62L antibodies. The findings of the competitive inhibition research indicated that the phagocytosis of DOX@SAL was significantly suppressed by excess CD62L antibodies. CLSM results were consistent with the FCM analyses (Figs. 3I and S7). In the DOX@SAL group, stronger DOX signals and DAPI signals were co-distributed in cell nucleus. Together, DOX@SAL is able to efficiently target inflammatory neutrophil cells for transporting DOX inside cells by specifically attachment to L-selectin on the surface of neutrophil cells.

The cytotoxic effect of DOX formulations against inflammatory neutrophils was evaluated with a CCK-8 test. Findings indicated that all DOX formulations suppressed neutrophil viability in a dose-dependent manner (Fig. 3J). Free DOX showed the most potent inhibition capacity and was used as a positive control. DOX@SAL displayed a stronger cytotoxicity compared to DOX@CL, suggesting that the SA-PG-C18 modification augments the restraining impact of DOX-loaded liposomes against inflammatory neutrophils. The suppressing influence of DOX formulations against the chemotactic ability of inflammatory neutrophils was evaluated using a Transwell migration test (Fig. 3K). A gradient of chemical for neutrophil movement was generated via supplementing fMLP in the lower chamber [58]. Compared to the control group, The quantity of migrated inflammatory neutrophils into the lower chamber was significantly increased in the fMLP-added group. DOX formulations effectively suppressed the chemotactic ability of neutrophils, and the number of migrated neutrophils incubated with DOX@SAL resulted in a notably decreased amount compared to DOX@CL (Fig. 3L). These results suggest that SA-derivatized DOX-loaded liposomes possess effective anti-inflammatory properties and have the potential to reduce postoperative inflammation.

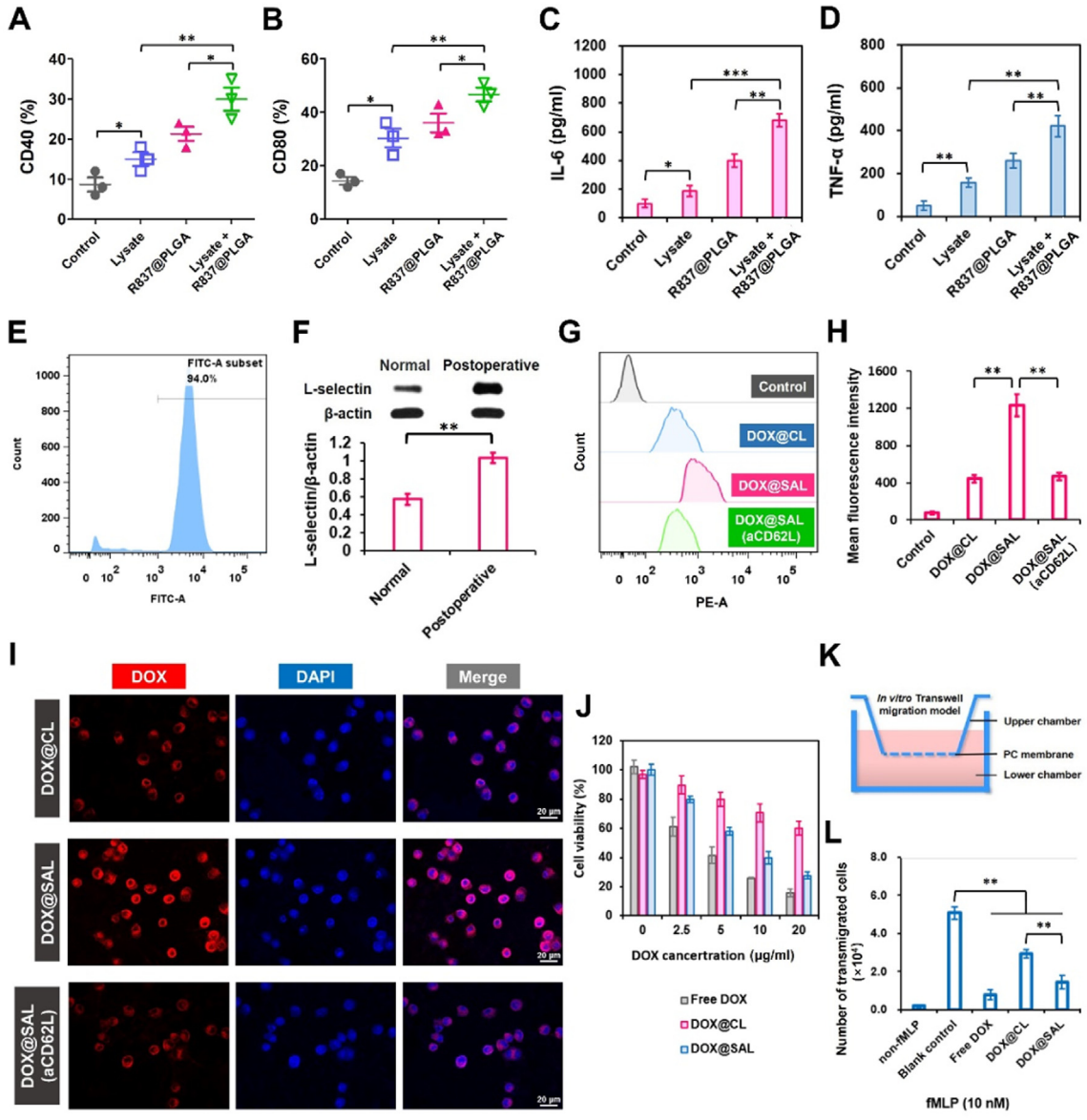

Fig. 3 – *In vitro* stimulation and maturing of BMDCs by S-CV, targeting and inhibition of neutrophils by DOX@SAL. (A) Percentage of CD11c$^+$CD40$^+$ and (B) CD11c$^+$CD80$^+$ BMDCs treated with tumor lysates and/or R837@PLGA; Concentrations of (C) IL-6 and (D) TNF-α produced from BMDCs treated with tumor lysates and/or R837@PLGA; (E) Degree of FITC-Gr-1 staining in isolated neutrophils; (F) L-selectin expression level on normal and inflammatory neutrophils investigated by western blot; (G) Uptake of liposomal DOX by inflammatory neutrophils analyzed using FCM. In competitive inhibition experiments, inflammatory neutrophils were pre-incubated using anti-CD62L mAb, subsequently cultured with DOX@SAL [called DOX@SAL (aCD62L) group]; (H) Quantitative analysis of the FCM results; (I) CLSM pictures of inflammatory neutrophils subjected to DOX@CL and DOX@SAL (red) incubation. DAPI was employed for nuclear staining (blue), scale bar = 20 μm; (J) Cell viability of inflammatory neutrophils treated with various DOX formulations analyzed using CCK-8 assay; (K) Schematic diagram of the Transwell migration assay; (L) Number of migrated neutrophils with internalized DOX preparations with or without fMLP. Results are mean ± SD, $n = 3$. ***$P < 0.001$, **$P < 0.01$, *$P < 0.05$.

3.5. *In vivo cytokine secretion and immune cell recruitment after surgery*

Initially, the ELISA test was utilized to quantify the secretion of chemotactic factors (TNF-α, CXCL1, and CCL2) associated with neutrophil and DC migration after surgery and S-CV implantation, including control groups without scaffold implantation or with blank scaffold implantation. Samples were collected on 0, 1, 2, 3, 4, and 5 d (Fig. 4A). Fig. 4B and 4C revealed significantly higher CXCL1 and TNF-α levels in the blood of all postoperative mice with neoplasm compared to those without surgery (***$P < 0.001$). The increased amounts of pro-inflammatory cytokines were attributed to the tumor removal process, which ultimately led to the

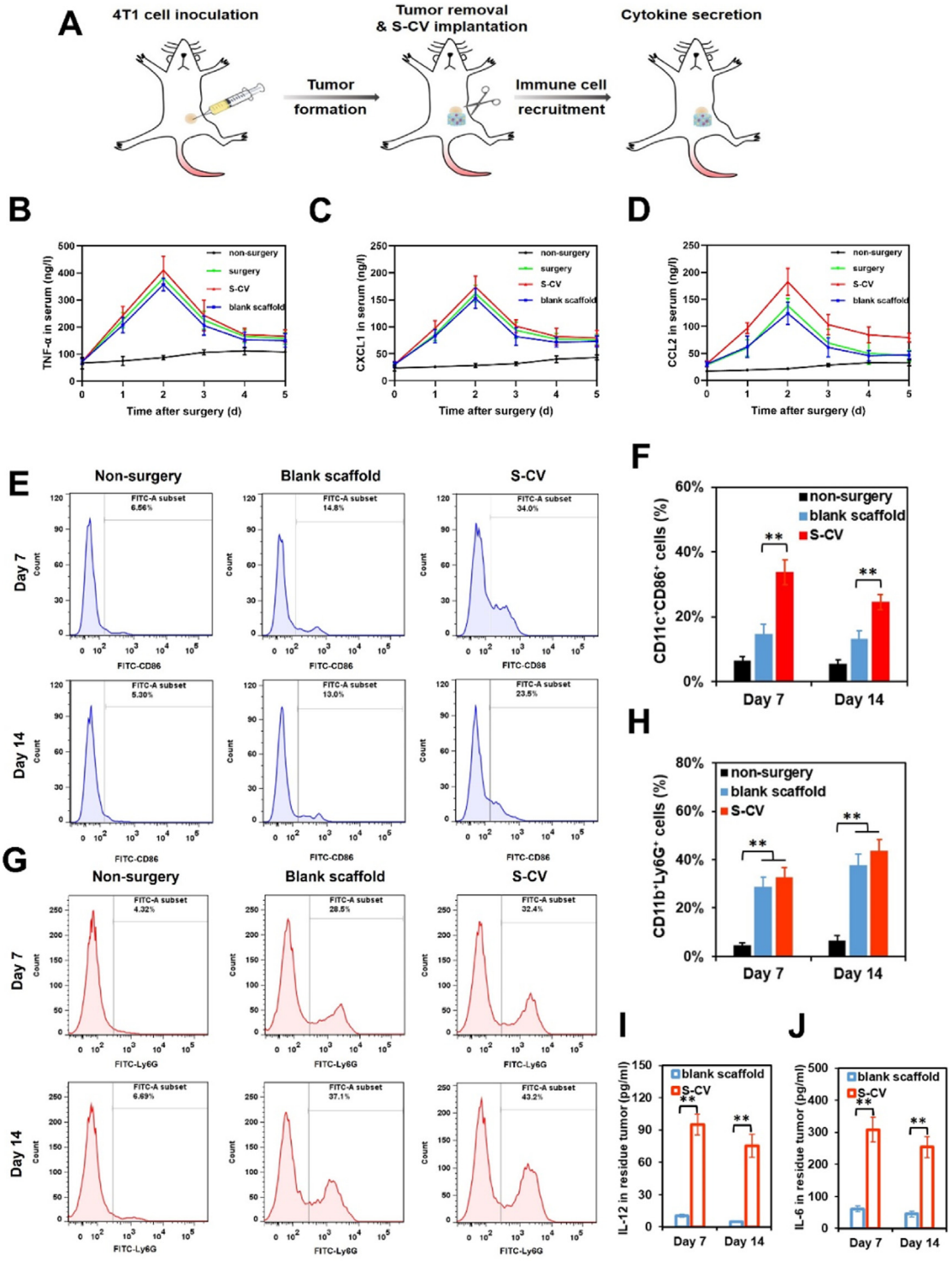

Fig. 4 – Tumor removal and S-CV implantation led to cytokine secretion and immune cell recruitment. (A) Schematic diagram illustrating the procedure of tumor removal and S-CV implantation; (B) TNF-α, (C) CXCL1 and (D) CCL2 levels in the blood of mice following surgery and scaffold implantation; The infiltration of (E-F) DCs ($CD11c^+CD86^+$) and (G-H) neutrophils ($Gr\text{-}1^+$) in the regrown tumor tissues after surgery and scaffold implantation; The concentrations of (I) IL-12 and (J) IL-6 in the residual tumor tissues after surgery and scaffold implantation. "Non-surgery" referred to tumor-bearing mice that did not undergo surgery and was used as a control group for the surgical group. Results are mean ± SD, $^{**}P < 0.01$, $n = 3$.

chemotactic migration of inflammatory neutrophils [59,60]. The chemotactic factor CCL2 is involved in DC migration [61]. As depicted in Fig. 4D, surgery upregulated CCL2 production in the blood of mice with neoplasm ($^{**}P < 0.01$). Furthermore, the S-CV group exhibited a significantly higher CCL2 level compared to the blank scaffold implantation group and without scaffold implantation group ($^{*}P < 0.05$), indicating that a systemic DC-recruitment immune response was induced by the gradual release of the vaccine. No significant distinction was shown in the concentrations of cytokines TNF-α, CXCL1, and CCL2 on postoperative Day 5 compared with Day 0, suggesting that the inflammatory response mediated by the surgical procedure had gradually returned to normal by this time.

To investigate the ability of porous networks containing vaccines to recruit and activate antigen-presenting cells, S-CV and blank scaffolds were implanted adjacent to residual tumor tissues and harvested on Day 5, 7, 14 and 30 after surgery. As depicted in Figs. 4E-4F and S8A-S8B, S-CV markedly elevated the migration of DCs within the porous networks when contrasted with the blank scaffold implantation group and without scaffold implantation group. Additionally, the gradual release of tumor cell lysates and R837@PLGA led to significantly elevated release of IL-6 and IL-12 into the surrounding tumor tissues, which were released by the matured and activated DCs at the S-CV implantation sites [62] (Figs. 4I-4J and S8C-S8D). These findings suggest that scaffolds loaded with tumor antigens and immune adjuvants can efficiently recruit and activate DCs, thereby triggering a systemic anti-tumor immune response.

However, tumors often employ various strategies, including recruiting immunosuppressive cells, to enhance the intricacy of the tumor's immune milieu and escape anti-tumor immunity. It is noteworthy that postoperative inflammatory responses, along with the pro-inflammatory factors released by activated DCs, can recruit a significant quantity of inflammatory neutrophils to the sites of neoplasms. This recruitment poses various challenges to the success of vaccine-mediated immunotherapy [26,63]. To identify treatment targets and probe immunosuppressive mechanisms, the infiltration of inflammatory neutrophils was further investigated. As shown in Fig. 4G and 4H, the increased amounts of inflammatory neutrophils and decreased amounts of DCs on Day 14 and 30 compared to Day 5 and 7 in residual tumor tissues of all postoperative tumor-bearing mice ($^{*}P < 0.05$, Fig. 4E and 4F) suggest that targeting and subsequent inhibition of inflammatory neutrophils would improve anti-tumor immunotherapy.

3.6. *DOX@SAL improves postoperative tumor immunotherapy based on S-CV*

S-CVs were implanted into residual 4T1 tumors to modulate the immunosuppressive neoplastic environment, as well as the influence of inflammatory neutrophil blockade on postoperative cancer therapy was also investigated. As illustrated in Fig. 5A, neoplastic cells (4T1, 1×10^6 per mouse) were subcutaneously inoculated in the mammary adipose tissue of female BALB/c mice, and surgical procedures were performed when the tumor dimensions attained approximately 200 mm^3. About 10% the original neoplasm tissues were remaining for simulating the incomplete tumor removal state in clinical settings. Porous scaffolds were implanted during the surgical procedure, and DOX-loaded liposomes were administered intravenously 24 h after tumor resection. The combined therapeutic efficacy of scaffolds and liposomal DOX was evaluated by measuring the tumor mass, as well as viability time of mice.

During the experiment, tumor weights of mice treated only with surgery or blank scaffolds continued to increase, while their body weights decreased significantly. No mice within the control and blank scaffold groups survived for more than 25 d after surgery, indicating that tumor resection alone is insufficient due to recurrence and metastasis. In addition, there were no remarkable differences between the DOX@CL and control groups, likely because liposomal DOX was delivered at a very low dosage of 0.5 mg/kg compared to the conventional DOX dose of 5 mg/kg used in cancer chemotherapy [64]. However, mice implanted with S-CV or injected with DOX@SAL showed a notable reduction in tumor weight, a slow decrease in body weight, and death within 35 d after surgery. These results demonstrated the tumor microenvironment-modulating effect of S-CV and the inflammatory neutrophil inhibitory ability of DOX@SAL. The treatment containing both S-CV and DOX@CL markedly diminished the rate of tumor advancement and mice death compared to monotherapies, Suggesting the enhanced impact of combined treatment. Remarkably, 62.5% of mice in the S-CV plus DOX@SAL group were free of regrowth tumors, survived for more than 50 d, and had a slow and stable increase in body weight. These findings suggest that the significant inflammatory neutrophil inhibitory property of DOX@SAL is crucial for enhancing the S-CV-mediated postoperative immunotherapy in 4T1 breast cancer mouse models (Figs. 5B-5E and S9- S10).

Inflammatory neutrophils have been reported to be recruited to the "pre-metastatic niche" and promote distant tumor growth, and blocking their accumulation has been found to inhibit spontaneous cancer metastasis [28,65,66]. Therefore, lung metastasis was evaluated to further investigate the efficacy of the combination therapeutic strategy. As shown in Figs. 5F-5G and S11, counting of secondary tumor formations and histological H&E analysis of lungs harvested 28 d after surgery confirmed that the tumor metastatic rate was significantly reduced in the S-CV plus DOX@SAL group compared to other treatment groups. Biosafety was also a major concern in postoperative cancer therapy, and histological examination of vital tissues in mice was conducted following diverse interventions. As shown in Fig. S12, unlike DOX solution (i.v. 5 mg/kg) administration, which caused obvious cardiotoxicity, the local treatment using S-CV and the systemic treatment using liposomal DOX at an extremely low dosage of 0.5 mg/kg had no apparent toxic effects on the liver, heart, kidney and spleen.

To further evaluate the antitumor immunity generated by the drug combinations in the pharmacodynamic study, immune cell profiling and cytokine production within the tumor tissues and major immune organs after various treatments were analyzed to determine the changes in the tumor's immunological response. The DC population from

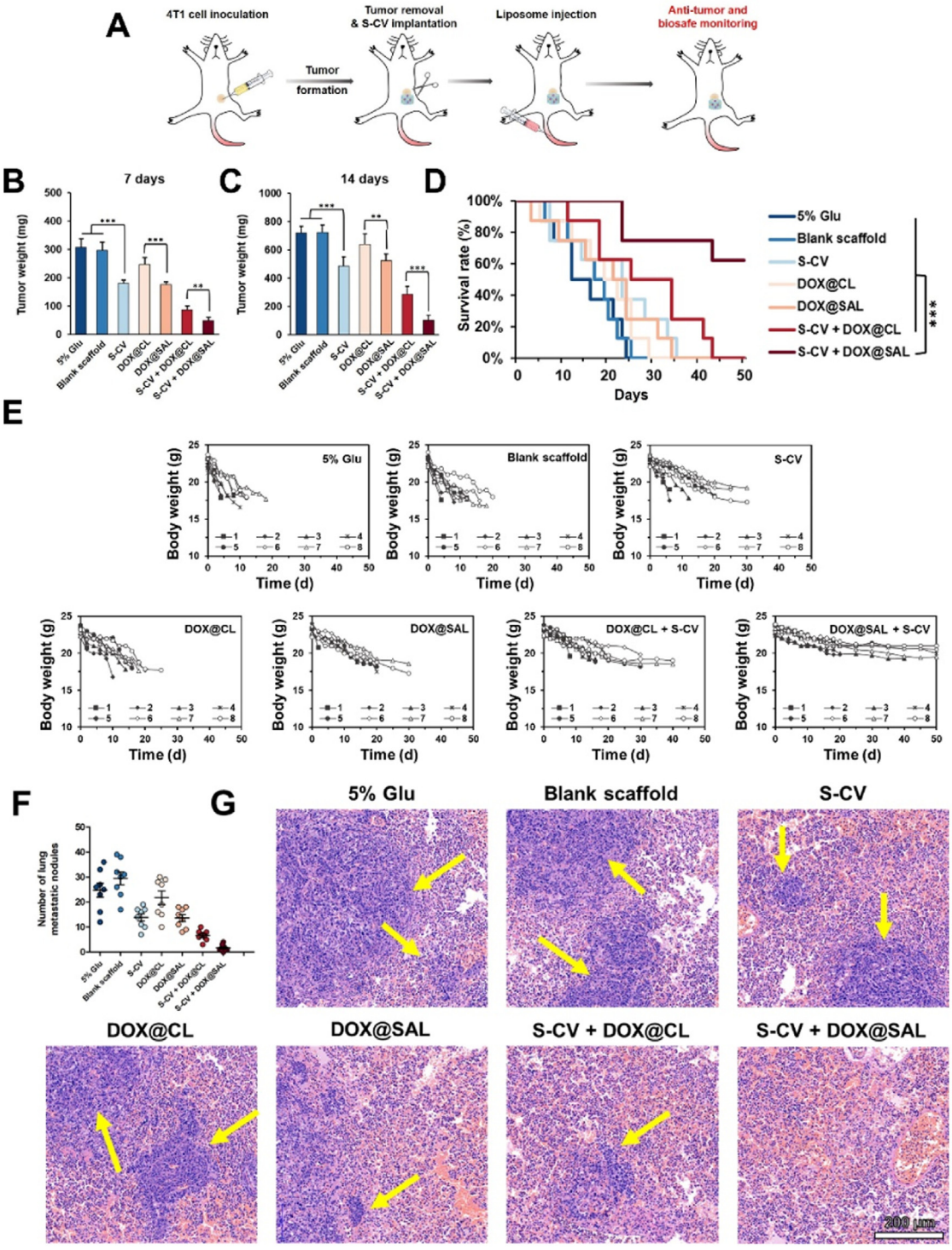

Fig. 5 – The synergistic impact of combined treatments in murine models on tumor suppression. (A) Treatment regimen for combined therapy utilizing S-CV and liposomal DOX. Scaffolds were implanted with 500 μg tumor lysate protein and 100 μg of R837 per mouse. DOX formulations were administered intravenously with a dose of 0.5 mg/kg; Tumor weights on (B)Day 7 and (C) Day 14 after tumor resection following different treatments; (D) Survival rate of postoperative mice following varied interventions; (E) Changes in body weight of postoperative mice following different treatments; (F) Metastasis inhibition via different treatments in postoperative mouse models with neoplasms; (G) H&E study of the pulmonary tissue on Day 28 after tumor resection, the yellow arrow pointed to the metastatic node, scale bar = 20 μm. Results are average ± SD ($n = 8$), $^{**}P < 0.01$, $^{***}P < 0.001$.

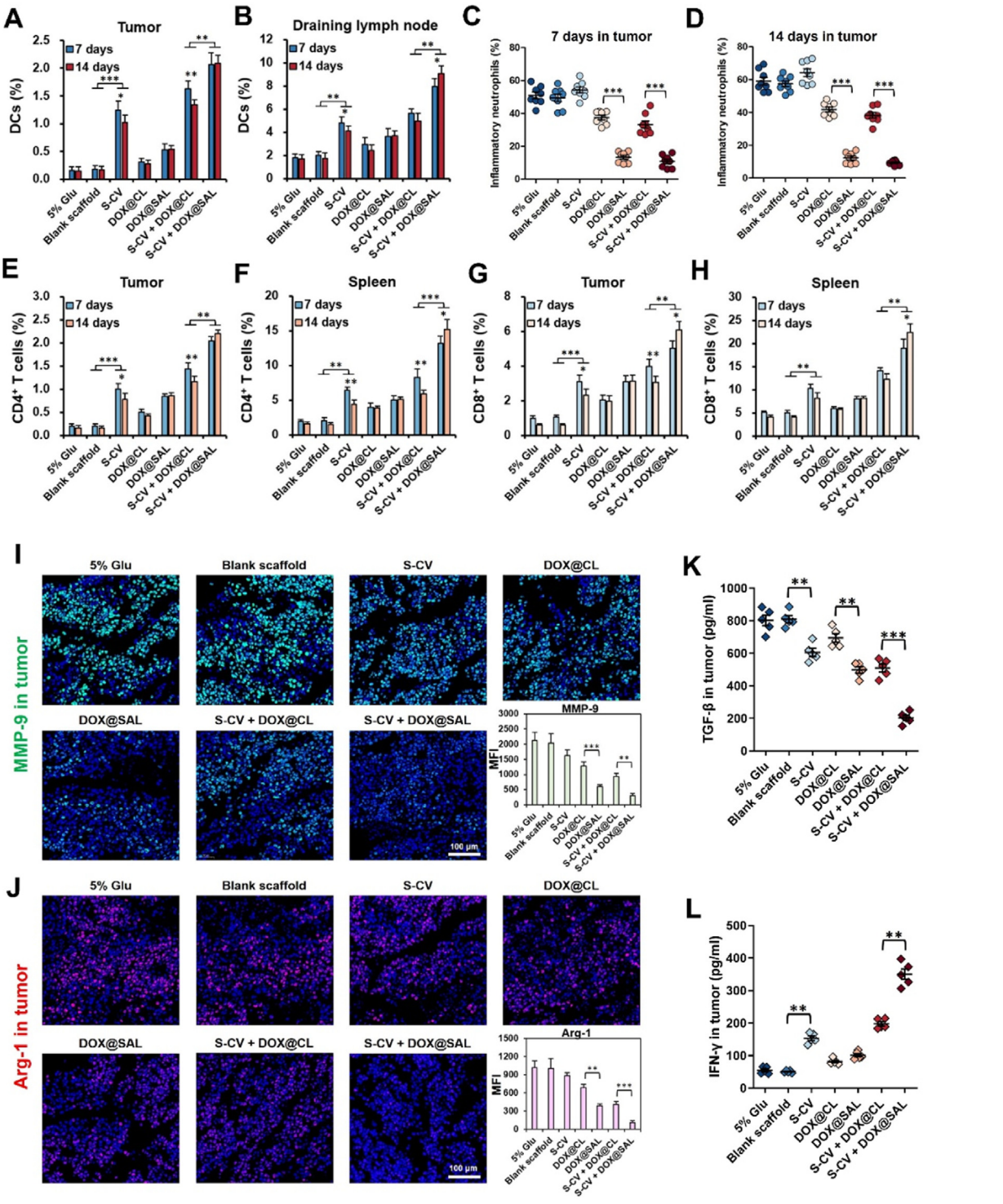

Fig. 6 – Immune response against cancer triggered by S-CV plus DOX@SAL in postoperative mice. The DC ($CD11c^+CD86^+$) population increased in (A) regrown tumors and (B) lymph nodes with S-CV-mediated immunotherapy; The inflammatory neutrophil ($Gr\text{-}1^+$) population decreased on (C) Day 7 and (D) Day 14 with DOX@SAL-mediated combined therapy. The proportion of (E) $CD4^+$ T cells in neoplasm and (F) spleens, (G) $CD8^+$ T cells in tumors, and (H) spleens after various treatments (all gated on $CD3^+$ lymphocytes); Typical immunofluorescence pictures of neoplasm sections stained with (I) FITC-MMP-9 (green) and (J) PE-Arg-1 (red); Cellular nuclei were labeled using DAPI (blue), scale bar = 20 μm; ELISA analysis of the intratumoral release of (K) TGF-β and (L) IFN-γ after the various treatments. Results are average ± SD, $n = 8$. $^{***}P < 0.001$, $^{**}P < 0.01$.

tumor-draining lymph nodes, as well as neoplasms, was first quantified on 7 and 14 d after tumor resection. As shown in Fig. 6A and 6B, mice treated with S-CV-mediated monotherapies and combined therapies all presented a marked increase in DC population in contrast to the control group, implying that the local implantation of S-CV could trigger a systemic presentation of neoplasm antigens. The intensity of the immune response against malignancy can usually be indicated through the frequency of effector T cells proliferating and infusing within the spleens and tumors [67,68]. A marked elevation in the $CD8^+$ and $CD4^+$ T cell populations was observed in the S-CV-mediated monotherapy and combined treatment groups in the first week, while slightly decreased in the second week, perhaps due to the adverse effects of the postoperative inflammatory response on antitumor immunity (Fig. 6E-6H).

Reportedly, continuous infiltration of inflammatory neutrophils at the postoperative tumor site accelerates the excretion of cytokines that support tumor development, including Arg-1 and MMP-9, which are closely related to immunosuppression and tumor recurrence [69,70]. As shown in Fig. 6C and 6D, the intratumoral density of neutrophils treated with DOX@SAL-mediated monotherapies and combined therapies was significantly lower than that of other groups. In addition, the transcript level (Fig. S13) and intratumoral expression (Fig. 6I and 6J) of Arg-1 and MMP-9 were significantly decreased after DOX@SAL-included treatments. These results suggested that SA-modified liposomal DOX can effectively suppress the penetration and tumor-promoting role of inflammatory neutrophil cells in the postoperative tumor sites. Most importantly, the inhibition of inflammatory neutrophils greatly enhanced the effector cell populations. The highest $CD8^+$ and $CD4^+$ T cell frequencies were observed in S-CV plus DOX@SAL treatment group from the initial week and persisted at a relatively high level up to the second week (Fig. 6E-6H). Moreover, cytokine TGF-β was reported to participate in triggering immunosuppressive functions by tumor-associated neutrophils [71,72]. Compared to other therapy groups, a remarkable diminishment in TGF-β expression was observed in S-CV plus DOX@SAL group (Fig. 6K). Cytokine IFN-γ is crucial in antitumor immune response [73,74]. Combined treatment using S-CV and DOX@SAL significantly increased the secretion of IFN-γ compared to all other therapy groups (Fig. 6L). We evaluated the immunosuppressive cells in the recurrent neoplasm tissues using FCM. The results showed (Fig. S14) a substantial reduction in the quantity of M2 TAMs, Tregs, as well as M-MDSCs infiltrated in S-CV+DOX@SAL group compared with surgery mice. All data confirmed that DOX@SAL could greatly inhibit the infiltration and pro-tumor functions of inflammatory neutrophils, and the cascade reaction induced by these results markedly enhance the anti-tumor immunity mediated by S-CV, thereby suppressing tumor recurrence and metastasis.

4. Conclusion

In summary, this study introduces a novel chemoimmunotherapeutic approach by combining an implantable macroporous S-CV with a sialic acid derivative-decorated liposomal DOX (DOX@SAL) to enhance the efficacy of post-surgical treatment. The S-CV utilizes whole tumor lysates as antigens and R837-loaded PLGA nanoparticles as immunological adjuvants to provoke a robust anti-cancer immune reaction. Meanwhile, DOX@SAL specifically targets inflammatory neutrophils, reducing their recruitment and gathering at the postoperative neoplasm location, mitigating the immunosuppressive effects of postoperative inflammation, and enhancing the efficacy of localized tumor vaccine. However, in the future we still need further research to overcome the limitations of tumor heterogeneity, technological limitations, as well as cost and accessibility to improve the effectiveness of the combined strategy. The combined chemoimmunotherapeutic strategy demonstrates remarkable potential in suppressing local tumor recurrence and distant tumor development after surgery, with minimal systemic toxicity. This innovative approach highlights the potential of combining immunotherapy with targeted nanoplatforms to address the challenges of postoperative tumor treatment.

Conflicts of interest

The authors assert no financial conflicts or competing interests.

Acknowledgments

This research received funding from the Liaoning Province Doctoral Start-up (grant number 2023-BS-086).

Supplementary materials

Supplementary material associated with this article can be found, in the online version, at doi:10.1016/j.ajps.2024.100906.

REFERENCES

[1] Demicheli R, Retsky MW, Hrushesky WJ, Baum M, Gukas ID. The effects of surgery on tumor growth: a century of investigations. Ann Oncol 2008;19:1821–8.
[2] Chemi F, Rothwell DG, McGranahan N, Gulati S, Abbosh C, Pearce SP, et al. Pulmonary venous circulating tumor cell dissemination before tumor resection and disease relapse. Nat Med 2019;25:1534–9.
[3] Wang K, Zhang X, Ye H, Wang X, Fan Z, Lu Q, et al. Biomimetic nanovaccine-mediated multivalent IL-15 self-transpresentation (mist) for potent and safe cancer immunotherapy. Nat Commun 2023;14:6748.
[4] Liu C, He D, Li L, Zhang S, Wang L, Fan Z, et al. Extracellular vesicles in pancreatic cancer immune escape: emerging roles and mechanisms. Pharmacol Res 2022;183:106364.
[5] Yu YH, Wu X, Wang MY, Liu WJ, Zhang L, Zhang Y, et al. Optogenetic-controlled immunotherapeutic designer cells for post-surgical cancer immunotherapy. Nat Commun 2022;13:6357.

[6] Wang KY, Li Y, Wang X, Zhang ZJ, Cao LP, Fan XY, et al. Gas therapy potentiates aggregation-induced emission luminogen-based photoimmunotherapy of poorly immunogenic tumors through cgas-sting pathway activation. Nat Commun 2023;14:2950.
[7] Zeng FC, Fan ZJ, Li SY, Li LQ, Sun T, Qiu Y, et al. Tumor microenvironment activated photoacoustic-fluorescence bimodal nanoprobe for precise chemo-immunotherapy and immune response tracing of glioblastoma. ACS Nano 2023;17:19753–66.
[8] Fan ZJ, Wang YC, Li LQ, Zeng FC, Shang QP, Liao YH, et al. Tumor-homing and immune- reprogramming cellular nanovesicles for photoacoustic imaging-guided phototriggered precise chemoimmunotherapy. ACS Nano 2022;16:16177–90.
[9] Ban WY, Sun MC, Huang HW, Huang WX, Pan SW, Liu PF, et al. Engineered bacterial outer membrane vesicles encapsulating oncolytic adenoviruses enhance the efficacy of cancer virotherapy by augmenting tumor cell autophagy. Nat Commun 2023;14:2933.
[10] Waldman AD, Fritz JM, Lenardo MJ. A guide to cancer immunotherapy: from T cell basic science to clinical practice. Nat Rev Immunol 2020;20:651–68.
[11] Oiseth SJ, Aziz MS. Cancer immunotherapy: a brief review of the history, possibilities, and challenges ahead. J Cancer Metastasis Treat 2017;3:250–61.
[12] Hegde PS, Chen DS. Top 10 challenges in cancer immunotherapy. Immunity 2020;52:17–35.
[13] Viswanath DI, Liu HC, Huston DP, Chua CYX, Grattoni A. Emerging biomaterial-based strategies for personalized therapeutic *in situ* cancer vaccines. Biomaterials 2022;280:121297.
[14] Liu J, Liew SS, Wang J, Pu K. Bioinspired and biomimetic delivery platforms for cancer vaccines. Adv Mater 2022;34:e2103790.
[15] Shang Q, Dong Y, Su Y, Leslie F, Sun M, Wang F. Local scaffold-assisted delivery of immunotherapeutic agents for improved cancer immunotherapy. Adv Drug Deliv Rev 2022;185:114308.
[16] Obradovic AZ, Dallos MC, Zahurak ML, Partin AW, Schaeffer EM, Ross AE, et al. T-cell infiltration and adaptive treg resistance in response to androgen deprivation with or without vaccination in localized prostate cancer. Clin Cancer Res 2020;26:3182–92.
[17] Yang C, Blum NT, Lin J, Qu J, Huang P. Biomaterial scaffold-based local drug delivery systems for cancer immunotherapy. Sci Bull 2020;65:1489–504.
[18] Cai L, Xu J, Yang Z, Tong R, Dong Z, Wang C, et al. Engineered biomaterials for cancer immunotherapy. MedComm 2020;2020(1):35–46.
[19] Prestwich GD. Hyaluronic acid-based clinical biomaterials derived for cell and molecule delivery in regenerative medicine. J Control Release 2011;155:193–9.
[20] Ouellette JN, Drifka CR, Pointer KB, Liu Y, Lieberthal TJ, Kao WJ, et al. Navigating the collagen jungle: the biomedical potential of fiber organization in cancer. Bioengineering 2021;8:17.
[21] Meng J, Meng J, Duan J, Kong H, Li L, Wang C, et al. Carbon nanotubes conjugated to tumor lysate protein enhance the efficacy of an antitumor immunotherapy. Small 2008;4:1364–70.
[22] Chiang CL, Coukos G, Kandalaft LE. Whole tumor antigen vaccines: where are we? Vaccines 2015;3:344–72.
[23] Meng Z, Fang X, Fu B, Qian C, Yang Z, Bai Y, et al. Tumor immunotherapy boosted by r837 nanocrystals through combining chemotherapy and mild hyperthermia. J Control Release 2022;350:841–56.
[24] Wei X, Liu L, Li X, Wang Y, Guo X, Zhao J, et al. Selectively targeting tumor-associated macrophages and tumor cells with polymeric micelles for enhanced cancer chemo-immunotherapy. J Control Release 2019;313:42–53.
[25] Mantovani A, Allavena P, Sica A, Balkwill F. Cancer-related inflammation. Nature 2008;454:436–44.
[26] Greten FR, Grivennikov SI. Inflammation and cancer: triggers, mechanisms, and consequences. Immunity 2019;51:27–41.
[27] Wang Q, Zhu D. The prognostic value of systemic immune-inflammation index (sii) in patients after radical operation for carcinoma of stomach in gastric cancer. J Gastrointest Oncol 2019;10:965–78.
[28] Coffelt SB, Wellenstein MD, de Visser KE. Neutrophils in cancer: neutral no more. Nat Rev Cancer 2016;16:431–46.
[29] Shaul ME, Fridlender ZG. Tumour-associated neutrophils in patients with cancer. Nat Rev Clin Oncol 2019;16:601–20.
[30] Gregory AD, Houghton AM. Tumor-associated neutrophils: new targets for cancer therapy. Cancer Res 2011;71:2411–16.
[31] Chu D, Zhao Q, Yu J, Zhang F, Zhang H, Wang Z. Nanoparticle targeting of neutrophils for improved cancer immunotherapy. Adv Healthc Mater 2016;5:1088–93.
[32] Zhang Y, Guoqiang L, Sun M, Lu X. Targeting and exploitation of tumor-associated neutrophils to enhance immunotherapy and drug delivery for cancer treatment. Cancer Biol Med 2020;17:32–43.
[33] Ivetic A. A head-to-tail view of L-selectin and its impact on neutrophil behaviour. Cell Tissue Res 2018;371:437–53.
[34] Qiu Q, Li C, Song Y, Shi T, Luo X, Zhang H, et al. Targeted delivery of ibrutinib to tumor-associated macrophages by sialic acid-stearic acid conjugate modified nanocomplexes for cancer immunotherapy. Acta Biomater 2019;92:184–95.
[35] Wang S, Lai X, Li C, Chen M, Hu M, Liu X, et al. Sialic acid-conjugate modified doxorubicin nanoplatform for treating neutrophil-related inflammation. J Control Release 2021;337:612–27.
[36] Ding J, Sui D, Liu M, Su Y, Wang Y, Liu M, et al. Sialic acid conjugate-modified liposomes enable tumor homing of epirubicin via neutrophil/monocyte infiltration for tumor therapy. Acta Biomater 2021;134:702–15.
[37] Alifakioti D, Daccord C, Lachenal Y, Fitting JW. Acute eosinophilic and neutrophilic pneumonia following transarterial chemoembolization with drug-eluting beads loaded with doxorubicin for hepatocellular carcinoma: a case report. Respiration 2014;88:426–9.
[38] Islam MR, Patel J, Back PI, Shmeeda H, Adamsky K, Yang H, et al. Comparative effects of free doxorubicin, liposome encapsulated doxorubicin and liposome co-encapsulated alendronate and doxorubicin (plad) on the tumor immunologic milieu in a mouse fibrosarcoma model. Nanotheranostics 2022;6:451–64.
[39] Makwana V, Karanjia J, Haselhorst T, Anoopkumar-Dukie S, Rudrawar S. Liposomal doxorubicin as targeted delivery platform: current trends in surface functionalization. Int J Pharm 2021;593:120117.
[40] Borys N, Dewhirst MW. Drug development of lyso-thermosensitive liposomal doxorubicin: combining hyperthermia and thermosensitive drug delivery. Adv Drug Deliv Rev 2021;178:113985.
[41] Sebeke LC, Castillo Gomez JD, Heijman E, Rademann P, Simon AC, Ekdawi S, et al. Hyperthermia-induced doxorubicin delivery from thermosensitive liposomes via MR-HIFU in a pig model. J Control Release 2022;343:798–812.
[42] Shaldoum F, El-kott AF, Ouda MMA, Abd-Ella EM. Immunomodulatory effects of bee pollen on doxorubicin-induced bone marrow/spleen immunosuppression in rat. J Food Biochem 2021;45:e13747.
[43] Danhier F, Ansorena E, Silva JM, Coco R, Le Breton A, Preat V. Plga-based nanoparticles: an overview of biomedical applications. J Control Release 2012;161:505–22.

[44] Lin KF, He S, Song Y, Wang CM, Gao Y, Li JQ, et al. Low-temperature additive manufacturing of biomimic three-dimensional hydroxyapatite/collagen scaffolds for bone regeneration. ACS Appl Mater Interfaces 2016;8:6905–16.
[45] Huang Z, Li X, Zhang T, Song Y, She Z, Li J, et al. Progress involving new techniques for liposome preparation. Asian J Pharmaceut Sci 2014;9:176–82.
[46] Swamydas M, Luo Y, Dorf ME, Lionakis MS. Isolation of mouse neutrophils. Curr Protoc Immunol 2015;110 3.20.1-3.20.15.
[47] Ren L, Lim YT. Degradation-regulatable architectured implantable macroporous scaffold for the spatiotemporal modulation of immunosuppressive microenvironment and enhanced combination cancer immunotherapy. Adv Funct Mater 2018;28:47.
[48] Ungaro F, Biondi M, d'Angelo I, Indolfi L, Quaglia F, Netti PA, et al. Microsphere-integrated collagen scaffolds for tissue engineering: effect of microsphere formulation and scaffold properties on protein release kinetics. J Control Release 2006;113:128–36.
[49] Ji Z, Tan Z, Li M, Tao J, Guan E, Du J, et al. Multi-functional nanocomplex codelivery of Trp2 and R837 to activate melanoma-specific immunity. Int J Pharm 2020;582: 119310.
[50] Torrano AA, Herrmann R, Strobel C, Rennhak M, Engelke H, Reller A, et al. Cell membrane penetration and mitochondrial targeting by platinum-decorated ceria nanoparticles. Nanoscale 2016;8:13352–67.
[51] Alsaab HO, Alharbi FD, Alhibs AS, Alanazi NB, Alshehri BY, Saleh MA, et al. PLGA-based nanomedicine: history of advancement and development in clinical applications of multiple diseases. Pharmaceutics 2022;14:2728.
[52] Dudek AM, Martin S, Garg AD, Agostinis P. Immature, semi-mature, and fully mature dendritic cells: toward a dc-cancer cells interface that augments anticancer immunity. Front Immunol 2013;4:438.
[53] Li X, Feng Q, Cui F. *In vitro* degradation of porous nano-hydroxyapatite/collagen/plla scaffold reinforced by chitin fibres. Mater Sci Eng: C 2006;26:716–20.
[54] Xing J, Liu D, Zhou G, Li Y, Wang P, Hu K, et al. Liposomally formulated phospholipid-conjugated novel near-infrared fluorescence probe for particle size effect on cellular uptake and biodistribution *in vivo*. Colloids Surf B Biointerfaces 2018;161:588–96.
[55] Wang MZ, Xu Y, Xie JF, Jiang ZH, Peng LH. Ginsenoside as a new stabilizer enhances the transfection efficiency and biocompatibility of cationic liposome. Biomater Sci 2021;9:8373–85.
[56] Fujii S, Liu K, Smith C, Bonito AJ, Steinman RM. The linkage of innate to adaptive immunity via maturing dendritic cells *in vivo* requires CD40 ligation in addition to antigen presentation and CD80/86 costimulation. J Exp Med 2004;199:1607–18.
[57] Hata H, Sakaguchi N, Yoshitomi H, Iwakura Y, Sekikawa K, Azuma Y, et al. Distinct contribution of IL-6, TNF-alpha, IL-1, and IL-10 to T cell-mediated spontaneous autoimmune arthritis in mice. J Clin Invest 2004;114:582–8.
[58] Heit B, Liu L, Colarusso P, Puri KD, Kubes P. PI3K accelerates, but is not required for, neutrophil chemotaxis to fMLP. J Cell Sci 2008;121:205–14.
[59] Tohme S, Simmons RL, Tsung A. Surgery for cancer: a trigger for metastases. Cancer Res 2017;77:1548–52.
[60] Kolaczkowska E, Kubes P. Neutrophil recruitment and function in health and inflammation. Nat Rev Immunol 2013;13:159–75.
[61] Jimenez F, Quinones MP, Martinez HG, Estrada CA, Clark K, Garavito E, et al. Ccr2 plays a critical role in dendritic cell maturation: possible role of CCL2 and NK-kB. J Immunol 2010;184:5571–81.
[62] Jung MY, Son MH, Kim SH, Cho D, Kim TS. IL-32gamma induces the maturation of dendritic cells with Th1- and Th17-polarizing ability through enhanced IL-12 and IL-6 production. J Immunol 2011;186:6848–59.
[63] Yao D, Dong M, Dai C, Wu S. Inflammation and inflammatory cytokine contribute to the initiation and development of ulcerative colitis and its associated cancer. Inflamm Bowel Dis 2019;25:1595–602.
[64] Bielack SS, Erttmann R, Winkler K, Landbeck G. Doxorubicin: effect of different schedules on toxicity and anti-tumor efficacy. Eur J Cancer Clin Oncol 1989;25:873–82.
[65] Wculek SK, Malanchi I. Neutrophils support lung colonization of metastasis-initiating breast cancer cells. Nature 2015;528:413–17.
[66] Tuting T, de Visser KE. Cancer. How neutrophils promote metastasis. Science 2016;352:145–6.
[67] Thommen DS, Schumacher TN. T cell dysfunction in cancer. Cancer Cell 2018;33:547–62.
[68] Liu YT, Sun ZJ. Turning cold tumors into hot tumors by improving T-cell infiltration. Theranostics 2021;11:5365–86.
[69] Singel KL, Segal BH. Neutrophils in the tumor microenvironment: trying to heal the wound that cannot heal. Immunol Rev 2016;273:329–43.
[70] Xiong S, Dong L, Cheng L. Neutrophils in cancer carcinogenesis and metastasis. J Hematol Oncol 2021;14:173.
[71] de Visser KE, Kast WM. Effects of TGF-beta on the immune system: implications for cancer immunotherapy. Leukemia 1999;13:1188–99.
[72] Shen Y, Lu C, Song Z, Qiao C, Wang J, Chen J, et al. Ursodeoxycholic acid reduces antitumor immunosuppression by inducing chip-mediated TGF-beta degradation. Nat Commun 2022;13:3419.
[73] Takeda K, Nakayama M, Hayakawa Y, Kojima Y, Ikeda H, Imai N, et al. IFN-gamma is required for cytotoxic T cell-dependent cancer genome immunoediting. Nat Commun 2017;8:14607.
[74] Shen J, Xiao Z, Zhao Q, Li M, Wu X, Zhang L, et al. Anti-cancer therapy with TNFalpha and IFNgamma: a comprehensive review. Cell Prolif 2018;51:e12441.